Advanced Sensor Research

ADVANCED SENSOR RESEARCH Open Access

www.advsensorres.com

RESEARCH ARTICLE OPEN ACCESS

Ammonia and Amine Responsive Conjugated Materials for Reusable Colorimetric Sensing

Ronja Thümmler[1] | Adriana Barros-Martínez[2] | Franziska S-C Lissel[1,2] | Emin Istif[2]

[1]Division Macromolecular Chemistry, Leibniz Institute of Polymer Research, Dresden, Germany | [2]Institute for Applied Polymer Physics, TU Hamburg, Hamburg, Germany

Correspondence: Franziska S-C Lissel (franziska.lissel@tuhh.de) | Emin Istif (emin.istif@tuhh.de)

Received: 3 November 2025 | **Revised:** 8 April 2026 | **Accepted:** 13 April 2026

Keywords: ammonia sensors | colorimetric sensors | conjugated polymers | organic dyes | organic synthesis

ABSTRACT

Ammonia and primary amines play indispensable roles in nature, agriculture, biology, and the chemical industry. Beyond their critical functions, they also serve as vital indicators in various applications, such as monitoring food spoilage, air pollution, and certain chronic diseases. Therefore, the development of novel materials for precise, simultaneous, and rapid detection of ammonia and amines is at the forefront of current research. In this study, we synthesized a series of π-conjugated materials containing cyclic maleic anhydride (MA) moieties, which provide reactive sites for ammonia/amine interaction, enabling colorimetric sensing. The materials were synthesized via green chemistry approaches without the use of metal catalysts or hazardous solvents. We investigated the colorimetric response of these materials toward ammonia and primary amines using optical spectroscopy and demonstrated their practical applicability by fabricating paper-based colorimetric assays. Notably, the color change induced by ammonia exposure was reversible upon treatment with acid, indicating the reusability of the sensor. This work presents a new class of sustainably synthesized materials as an alternative to conventional methods, offering a reusable sensing platform for colorimetric ammonia/amine detection.

1 | Introduction

Primary amines and ammonia play crucial roles in nature, agriculture, biological systems, and industry, where they serve as important precursors for many valuable everyday products [1, 2]. Despite their usefulness, excessive amounts of these compounds in the environment or food can pose potential hazards and adversely affect human health. For example, specific concentrations of total volatile basic nitrogen (TVB-N) are used as quality indicators in food, with acceptable levels being < 20 mg/100 g for fish, <15 mg/100 g for chicken, and <15 mg/100 g for beef. Higher concentrations can be toxic to humans [3]. Furthermore, although ammonia is a highly valuable industrial precursor, particularly in agriculture, human exposure should not exceed 25 ppm over 8 h to minimize its adverse effects [3]. In addition, excessive ammonia emissions contribute to soil acidification, which can lead to deforestation and the loss of agricultural land [4]. Therefore, selective detection of amine or ammonia-based chemicals is considered to be critically important in various fields to mitigate their potential adverse effects. Thus, the development of novel materials for the detection of these compounds remains at the forefront of scientific research.

Previous studies on amine and ammonia sensing have employed various detection techniques, including colorimetric, resistive, capacitive, and electrochemical methods. Although each approach provides a specific advantage for ammonia/amine sensing, the main research particularly focuses on (i) achieving low-level detection in the ppb range, (ii) high selectivity, and (iii) cost-effective sensor fabrication. Among these methods, colorimetric

sensors offer critical advantages, such as low detection limits, low production costs, and practical applicability in everyday use. Moreover, they can be readily adapted for various applications, including food quality monitoring and environmental sensing.

Colorimetric sensors exhibit their sensing response through a visible color change, enabling both a qualitative and quantitative evaluation, and for the former, eliminating the need for expensive and non-portable spectroscopic techniques to analyze the results. This color change can be observed in various materials, including organic and inorganic dyes, polymers, and metal nanoparticles and quantum dots, when exposed to amines or ammonia. Sensing mechanisms include acid–base chemistry, complexation, or charge transfer interactions [5]. Among the aforementioned materials for colorimetric sensing, inorganic nanoparticles and quantum dots must be used with caution due to their potential toxicity [6], and their practical applications–particularly in food or biological sensing –are therefore very limited. Contrastingly, organic dyes and polymers are particularly advantageous due to their lower toxicity, as well as their tunable molecular structures, which allow for precise modification of optical properties (such as absorption and emission). In this way, both the detection limit and selectivity of ammonia/amine sensors can be significantly improved. However, especially for the mass production of sensors, using sustainable strategies for the synthesis of conjugated materials is equally as important as tuning their optical and electronic properties. Yet, traditional synthesis relies heavily on carbon-carbon (C—C) coupling reactions, which often require metal catalysts, extended reaction times, and hazardous reagents.

The organic dye–based colorimetric sensors [5, 7–9] reported in literature are often characterized by specially designed molecules that incorporate π-conjugated structures along with functional groups capable of optical changes upon interaction with analytes. These functional groups can interact with analytes by acid–base reaction, or through the formation of charge-transfer complexes, in which the molecular dyes act as electron acceptors for amines. Both mechanisms result in a change in the absorption or emission spectrum, which serves as a measurable and often quantitative sensing parameter. Furthermore, studies on polymeric sensors have demonstrated that polymeric materials that do not absorb light can function as effective colorimetric sensors for amines or ammonia when integrated with suitable colorimetric indicators [10–12]. Additionally, conjugated linear polymers [1, 3, 13] and covalent organic [14, 15] or metal frameworks [16] (COFs or MOFs, respectively) have been reported as colorimetric or fluorometric sensors. Their structure is designed in a similar way to organic dyes to alter their optical properties by the presence of amine species. Although the reported approaches provide valuable insights into ammonia and amine sensing, to the best of our knowledge, the direct covalent linkage of ammonia or primary amines to conjugated structures of dyes or polymers has not yet been reported as a colorimetric sensing mechanism. Such an approach could yield a stable sensor capable of operating in humid environments, which is one of the main drawbacks of conventional colorimetric sensors, and, in addition to a visible color change, they could also exhibit altered electronic properties resulting from structural modification.

In this work, we report easy-to-synthesize amine-responsive materials that constitute of cyclic MA functionality using the Perkin reaction as a green and environmentally friendly synthetic approach. The resulted MA-based materials were characterized using nuclear magnetic resonance (NMR), infrared (IR), and ultraviolet–visible (UV–Vis) spectroscopy. Moreover, their reactivity towards ammonia and methylamine was systematically investigated by UV–vis spectroscopy, as cyclic MAs are highly reactive towards primary amines and ammonia. The observed changes in absorption characteristics demonstrate that MA-based materials are promising candidates for use in colorimetric sensing, offering great potential for the design of sensitive and selective sensors applicable in environmental, food, and healthcare fields.

2 | Result and Discussion

2.1 | Synthesis and Structural Characterization

The ammonia/amine-responsive materials were synthesized via the Perkin reaction, performed under the conditions shown in Scheme 1. The reactions described in this work involve the condensation of aryl vinyl mono- or di-glyoxylic acids with p-phenylenediacetic acid (PDA), which serves as the aryldiacetic acid component, where both functional groups (glyoxylic acids and acetic acid) undergo ring-closure reaction to form cyclic MA structures. While monoaldehydes were used to synthesize a small cyclic MA-based molecular dye as a model compound (MC), dialdehyde derivatives were employed in polycondensation reactions to produce materials P1 and P2, which have multiple repeating units of the MC derivative, resulting in conjugated oligomeric or polymeric structures. The glyoxylic acid derivatives were synthesized through an aldol condensation, and detailed synthetic procedures and characterizations are provided in the Supporting Information file (Schemes S2 and S3; Figures S1–S5). Additionally, 9-(2-ethylhexyl)carbazole-3,6-dicarbox-aldehyde and thieno[3,2-b]-thiophene-2,5-dicarboxaldehyde were tested for the synthesis of the corresponding glyoxylic acid derivatives, however, under the same reaction conditions, these reactions were unsuccessful (Scheme S4).

For the synthesis of the MC, a previously reported synthetic protocol [17] was employed. Details of synthesis and characterizations are provided in the Supporting Information (Figures S6 and S7). For the synthesis of P1 and P2, a microwave-assisted polycondensation reaction was conducted. For this polycondensation reaction, ^{1}H NMR characterization revealed that shorter reaction times of 10 and 30 min, as well as solvent-free conditions, did not yield any product (Figure S8). Therefore, to ensure polycondensation, the reaction time was increased to 2 h, and a minimal amount of 2-methyltetrahydrofuran (2-Me-THF) was introduced as a solvent to promote the growth of the repeating units. The use of a limited solvent volume was intentional to eliminate macrocyclization reactions via the Perkin condensation as previously reported [18]. At the end of the polycondensation reactions, the final products were easily isolated and purified. Details of the synthesis and characterizations are provided in the Supporting Information (Figures S6 and S7). Upon obtaining the MA-based compounds (MC, P1, and P2), we observed that MC exhibited better solubility than P1 and P2. This result was expected, as MA-based aromatic compounds are well known

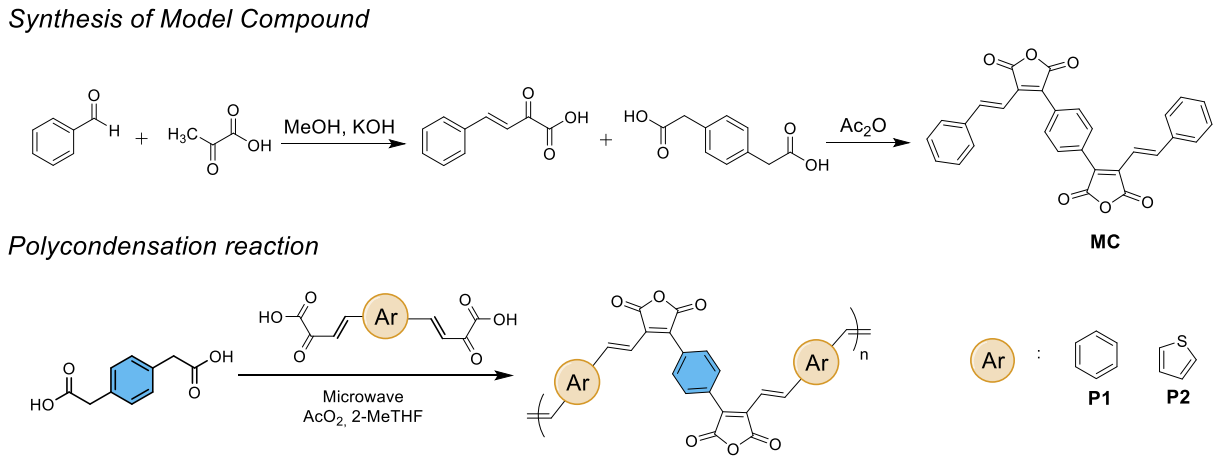

SCHEME 1 | Schematic illustration of the Perkin condensation reaction pathway for MC, P1, and P2.

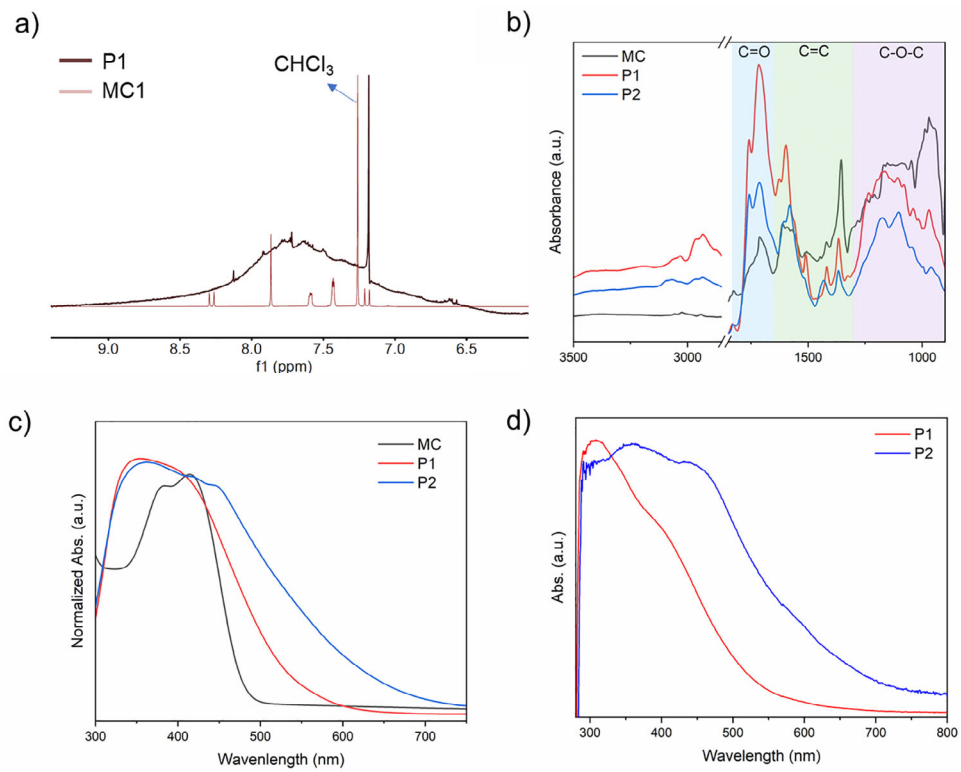

FIGURE 1 | (a) ^{1}H NMR spectra of P1 and MC-1, recorded in DMSO- d_6 and deuterated chloroform ($CDCl_3$), respectively, (b) Solid-state FTIR spectra of the synthesized samples. Comparison of UV-vis spectroscopy results of samples in tetrahydrofuran (THF) solution with the concentration of 00625 mg/mL (c), and in thin film (d).

for their poor solubility, especially in high molecular weight compounds [19].

To elucidate the structures of the synthesized materials, FTIR spectroscopy and NMR spectroscopy were employed for each sample. The ^{1}H and ^{13}C NMR spectra of MC are shown in Figures S6 and S7, respectively, and both spectra confirm the structure of MC. P1 and P2 were also investigated to gain insight into the structures of the MA-based polymeric species. The ^{1}H NMR spectrum of P1 was analyzed in comparison with its corresponding model compound, MC (Figure 1a and Figure S9). P1 exhibited very broad peaks in the aromatic region (6–9 ppm), suggesting extended conjugation, and slow molecular motion due to its complex and rigid structure [19, 20]. Additionally, the limited solubility of P1 in deuterated dimethylsulfoxide (DMSO-d_6) likely contributes to the broadening of the aromatic signals. To improve solubility, the ^{1}H NMR spectra of P1 were recorded at 60°C, 80°C, and 100°C (Figures S10 and S11). However, increasing the temperature did not result in improved results. Similarly, the ^{1}H NMR spectrum of P2 showed broad aromatic peaks in the

same region (6–9 ppm) (Figure S12). However, these signals were even less interpretable due to the lower solubility of P2 compared to P1, further complicating the ^{1}H NMR spectrum analysis. In the spectra of both P1 and P2, a distinct and sharp signal at 7.2 ppm was observed. This well-resolved aromatic peak is attributed to the protons of the phenyl ring located between two maleic anhydride (MA) units, confirming the successful formation of the targeted structural element. Both P1 and P2 showed a broad signal around 12.5 ppm, typical of acidic protons (—OH or —COOH). This may arise from carboxylic acids formed by partial hydrolysis of MA units or from terminal —COOH groups introduced by phenyldiacetic acid end-capping.

Structural characterization of all synthesized materials was also carried out using FTIR spectroscopy. The solid-state FTIR spectrum of MC exhibits (Figure 1b) characteristic carbonyl (C═O) stretching vibrations with two peaks (asymmetric and symmetric) at 1760 cm^{-1} as a broad peak and 1714 cm^{-1} as a sharp peak, indicative of the targeted cyclic MA structure. A minor peak is also observed around 1825 cm^{-1}, which can be attributed to trace impurities such as acetic acid or acetic anhydride, consistent with observations in the ^{1}H NMR spectrum (the signal appears around 2 ppm). In addition, MC displays C═C stretching bands corresponding to aromatic phenyl groups, vinyl groups, and maleic anhydride groups are present in the region from 1615 to 1350 cm^{-1}. The C—O—C stretching vibrations of the cyclic anhydride ring are also evident between 1100 and 950 cm^{-1} as a broad peak, as previously reported in the literature [21]. The FTIR spectra of P1 and P2 exhibit similar features with only minor shifts in peak positions compared to MC (Figure 1b), particularly in the carbonyl, vinyl, and ether regions, consistent with the expected structures. A notable difference was the presence of a broad band around 3500–3000 cm^{-1}, which likely originates from terminal —COOH groups or partial hydrolysis/ring-opening of MA, in line with observations from the ^{1}H NMR spectra.

We also investigated the molecular weights of P1 and P2 using THF-based gel permeation chromatography (GPC). Due to the limited solubility of P1 and P2 in THF, only the soluble fractions could be analyzed, which, as expected, exhibited low molecular weight values (Figure S13) corresponding to either the dimer or possible cyclic structures of P1 and P2. The low solubility prevented the analysis of the higher weight fractions.

2.2 | Optical Properties

The optical properties of the synthesized materials were characterized using UV–vis absorption spectroscopy. This provides insight into the compounds' optical features, which arise from their conjugated structures. The absorption spectra of MC, P1, and P2 were measured in THF-solution, and P1 and P2 are additionally characterized in solid state as thin films on quartz glass substrates (Figure 1c,d).

The MC spectrum exhibited a broad absorption from 300 to 500 nm, with maxima at 380 and 415 nm (Figure 1c). The 380 nm band is attributed to the n–π^* transition of carbonyl groups, while the 415 nm band corresponds to the π–π^* transition, originating from extended conjugation in the aromatic rings and vinyl groups [22, 23]. The UV–vis spectrum of P1 in solution was compared with MC to better analyze the absorption characteristics (Figure 1c). From Figure 1c, it is evident that while the absorption of MC ends around 500 nm, P1 exhibits an extended absorption tail reaching up to 650 nm, indicating a longer conjugation length in P1. Additionally, the two absorption peaks observed in MC are shifted to shorter wavelengths in P1. This shift can be attributed to increased aggregation due to the higher molecular weight of P1, which may reduce solubility and result in a hypsochromic (blue) shift [24–26]. For the P2 sample in solution, similar absorption characteristics were observed, with P2 showing maximum absorption at approximately 360 and 440 nm. Notably, the absorption tail of P2 ranges nearly 100 nm longer than that of P1. This red shift is likely due to an even higher conjugation length or due to the increased presence of aggregates.

To examine the thin-film absorption properties, we spin-coated P1 and P2 from THF-solutions onto quartz glass substrates. The processing conditions are described in the Experimental Section, and the thin-film characterization using confocal microscopy is detailed in the Supporting Information.

The obtained P1 and P2 thin films had thicknesses in the range of 20–35 nm and were subsequently characterized using absorption spectroscopy (Figure 1d). Both solid-state measurements resulted in spectral features similar to those observed in solution. For P1, a blue shift of approximately 25 nm was noted in the solid state. This behavior may be attributed to unfavorable packing of the oligomer and polymer chains in the film, likely caused by their complex molecular structures. Such packing can hinder optimal π-electron delocalization, leading to a shift toward shorter wavelengths [27–30]. The absorption profiles of P2 in the solid state are similar to those in solution, without the blue shift observed for P1. This behaviour could be related to the longer chains that facilitate more favourable molecular packing in thin films, thereby promoting efficient electron delocalization [31, 32]. Again, the absorption tail is longer for P2 than for P1, hinting at (i) a larger conjugated system or (ii) extended aggregation, probably due to aggregates already being present in the spin coating ink.

2.3 | Amine Sensing Tests

2.3.1 | UV–vis Characterization

Since MAs react rapidly with primary amines, we evaluated the synthesized MA-based materials as colorimetric probes for volatile amines, testing responses to aqueous ammonia ($NH_{3(aq)}$) (30 wt.%) and to the primary amine methylamine [33–37]. To assess the materials' potential, we examined three formats: (i) solution, (ii) thin film, and (iii) paper-based sensors.

For solution tests, 2 mL of THF solutions of MC, P1, and P2 (0.0625 mg/mL) were placed in 1.00 cm quartz cuvettes. Standardized $NH_{3(aq)}$ (30 wt.%) solution was added initially in 1.0 µL aliquots. For MC, 1.0 µL $NH_{3(aq)}$ addition corresponds to approximately 30 equivalents of NH_3 per MA unit (details provided in Supporting Information), while maintaining a single phase (water $\leq$ 0.032 vol.%). This calculation is not directly applicable to P1 and P2, as their exact molecular weights cannot be precisely determined. To ensure comparable experimental conditions, the same amount of $NH_{3(aq)}$ was added to the P1 and

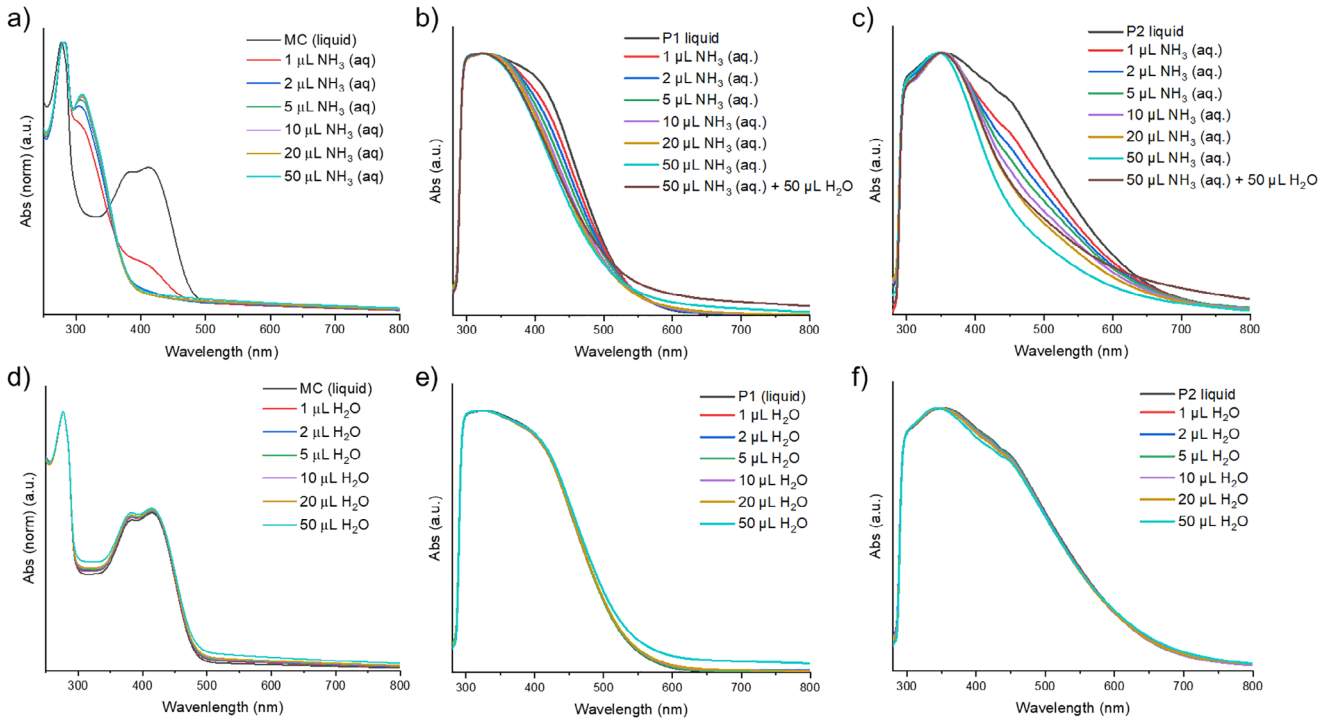

FIGURE 2 | Sensing studies: Changes in absorption of MC (a), P1 (b), and P2 (c) in THF-solution upon addition of $NH_{3(aq)}$. Changes in absorption of MC (d), P1 (e), and P2 (f) upon water addition.

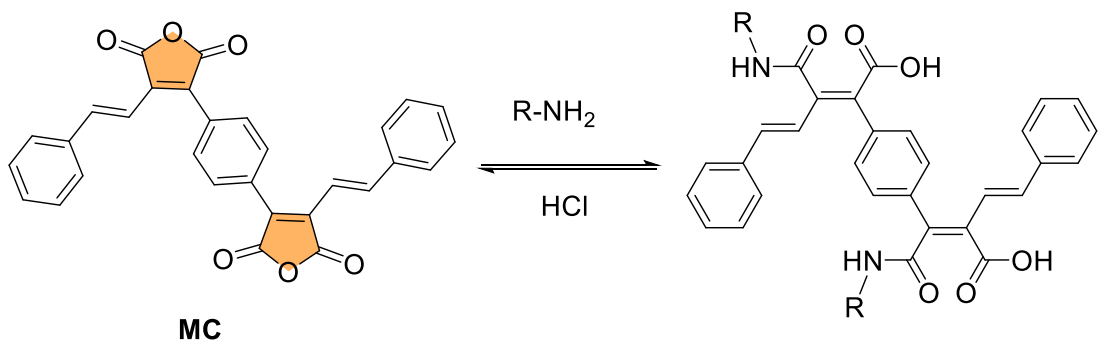

SCHEME 2 | Representative illustration of the reaction between primary amines and MC.

P2 solutions as used for MC. UV–vis spectra were recorded after each addition (Figure 2).

First, we investigated the absorption characteristics of the MC in the presence of $NH_{3(aq)}$. Upon the addition of a small amount of $NH_{3(aq)}$ (1 µL), the maximum absorption peak in the 390–450 nm range decreased by approximately 60% (Figure 2a). This decrease can be attributed to the disruption of the cyclic MA ring and the loss of conjugation, as this peak is associated with the π–π^* transition. Additionally, a new absorption peak appeared around 300 nm after the addition of $NH_{3(aq)}$, which can be ascribed to the n–π^* transition of the newly formed amide and carboxylic acid moieties, as illustrated in Scheme 2. The formation of carboxylic acid and amide moieties is also confirmed by FTIR characterization (Figure S25). Further addition of $NH_{3(aq)}$ (total volume 2 µL) resulted in the complete disappearance of the π–π^* transition, indicating that all the MA moieties had reacted with the used ammonia. The significant decrease in absorbance also demonstrates the high sensitivity of the sensor. Since absorbance is directly proportional to concentration, such a large change in absorbance with a very small amount of NH_3 suggests that the sensor could detect even much lower concentrations by showing a measurable response.

In the case of samples P1 and P2, the first absorption peak, which is related to the n–π^* -transition due to the presence of a carbonyl group of MA, does not change upon amine addition. However, the shoulder of the peak, in a wavelength range from 330 to 530 nm, starts to disappear (Figure 2b). At a wavelength of approximately 420 nm for P1 and 470 nm for P2, this change is the most pronounced. The addition of 1 µL of $NH_{3(aq)}$ also leads to a noticeable decrease in absorption of both P1 and P2. This change becomes more subtle with further additions of aqueous ammonia. Although P1 and P2 do not show as large a decrease

in absorption as MC, they are still capable of sensing less than 1 μL $NH_{3(aq)}$ and producing a measurable response, demonstrating that the materials are highly efficient and sense concentrations as low as 1 μL of $NH_{3(aq)}$. Additionally, the calibration curve for each sample was extracted (Figure S28), and the limit of detection (LOD) was calculated as 50.2 mM for MC, 20.8 mM for P1, and 2.10 mM for P2. The relatively high LOD for MC is attributed to the large decrease in absorbance observed after the addition of 1 μL of NH_3(aq); using a smaller amount of analyte could potentially improve the LOD for MC.

To exclude the influence of the solvent (water presence in $NH_{3(aq)}$), spectra were also recorded after adding pure water. Upon water addition, the absorption behavior of MC, P1, and P2 does not change up to an added volume of 20 μL (Figure 2d–f). However, adding a total of 50 μL water leads to an increased absorption at higher wavelengths above 530 nm for MC and P1, however, not in the case of P2. This can likely be attributed to aggregation of P1 and MC, as water is a poor solvent for both materials. In the case of P2, these aggregates are probably already present in the pristine THF solutions, as indicated by the more pronounced peak tailing. Lastly, we investigated whether water-induced aggregation affects sensing performance. Adding 50 μL water with 50 μL ammonium hydroxide (Figure 2b,c) increases the tail absorption of P1 and P2, but the decrease at 420 nm was only slightly affected, indicating that amine sensing capabilities are largely unaffected by water-induced aggregation.

Next, we tested solid-state sensing performance. Films obtained via spin-coating were exposed to different analytes by storing them in closed containers (50 mL) into which small amounts of different liquids were added (Figure S19). The concentration of NH_3 vapor (in ppm) was also calculated assuming complete evaporation of ammonia, and the details are provided in the Supporting Information. First, we tested the sensing of the P1 and P2 films against ammonia, and also studied varying the amount of ammonia vapor generated by vaporization of $NH_{3(aq)}$ at room temperature. The resulting data is presented in the Supporting Information. Again, the films exposed to $NH_{3(aq)}$ exhibited a decrease in absorption at the peak shoulder at higher wavelength (around 420 nm for P1, 490 nm for P2) (Figures S20 and S21). Initially, a smaller volume of 5 μL $NH_{3(aq)}$ leads to a less distinct change in the absorption peak than a volume of 20 μL, for both P1 and P2. Interestingly, when following the changes in absorption behavior of films exposed to different amounts of ammonia over time, we found that after one hour, the curves converged (Figures S20 and S21). This suggests that the reaction with the solid films is kinetically controlled, probably due to the vapor needing to diffuse into the solid films after reactive sites on the surface are converted completely.

Second, we also tested the films of P1 and P2 against the presence of methyl amine. Exposing P1 and P2 films to methyl amine led to a more pronounced decrease of absorption at 420 nm for P1, and 490 nm for P2, than exposing the sample to $NH_{3(aq)}$ vapor (Figures S22 and S23). This might be due to the +I-effect of the methyl group, leading to a destabilization of the nitrogen electron lone pair and, thus, higher reactivity. After 24 h, a difference between methyl amine and ammonia can still be observed, suggesting that different analytes exhibit different equilibrium states.

2.3.2 | Paper-Based Colorimetric Sensing

Finally, paper-based colorimetric sensors were prepared using the solution of synthesized materials (Figure 3d), as the paper-based approach provides a rapid and simple method to assess color changes in the presence of an analyte. Filter papers (Whatman, Ashless 541, 70 mm diameter) were cut into small pieces (1 cm × 1 cm), and 100 μL of each sample solution (2 mg/mL in THF) was drop-cast in five portions (fabrication details are given in the Supporting Information). Each piece of paper was then placed in a Petri dish and exposed to 20 μL of different chemicals ($NH_{3(aq)}$, ethanol, and water) for 10 min at room temperature. Photographs of the papers were taken under daylight using a smartphone (iPhone 11, Apple Inc., Cupertino, CA, USA; 12 MP rear camera, f/1.8 aperture) and are presented in their raw form (Figure S24) and as cropped rectangular images in Figure 3a.

To verify the selectivity of the paper-based colorimetric sensors, ethanol and water were also tested, as the ring-opening reaction of MA can occur in the presence of alcohols and water under certain conditions. Additionally, we further evaluated the selectivity of the sensor by testing acetone, ethyl acetate, and TEA as representative volatile compounds (Figures S26 and S27). The results demonstrated that a distinct color change was clearly visible to the naked eye when the paper-based sensors were exposed to $NH_{3(aq)}$. In particular, MC exhibited a pronounced color change upon $NH_{3(aq)}$ exposure, observable both visually and from RGB percentage plots. Although P1 and P2 did not show an obvious visual color change due to their inherently deep colors, the RGB intensity plots confirmed measurable differences. The color of all samples remained largely unaffected by ethanol and water, and other tested volatiles, suggesting that the sensors are selective for ammonia and primary amines, consistent with the structural transformation proposed in Scheme 2. We also observed that MC exhibits a strong emission feature under fluorescence excitation at 366 nm (Figure 3b–d), which disappears upon exposure of the film to ammonia vapor. This indicates that the material can be used as a fluorimetric sensor as well.

Additionally, the reversibility of the color change was demonstrated by exposing the $NH_{3(aq)}$-exposed paper samples to hydrochloric acid (HCl) (37%). Since the ring-opening reaction of MA in the presence of amines, ammonia, or bases can be reversed by acid treatment to reform the cyclic MA ring, this process enables sensor recovery for multiple uses. As shown in Figure 3c–e, the color recovery–particularly for MC–was clearly visible to the naked eye and confirmed by RGB percentage analysis. Additionally, the acetone solution of MC was first treated with 20 μL of ammonia. Upon the immediate color change from yellow to transparent, approximately 50 μL of 50% HCl (37%) was added, resulting in a yellowish, turbid solution, as shown in Figure 3e. The observed turbidity is attributed to the neutralization reaction between ammonia and HCl, forming ammonium chloride, which is insoluble in organic solvents. These observations support the reaction mechanism illustrated in Scheme 2 and demonstrate the recyclability of the proposed colorimetric sensors for repeated applications.

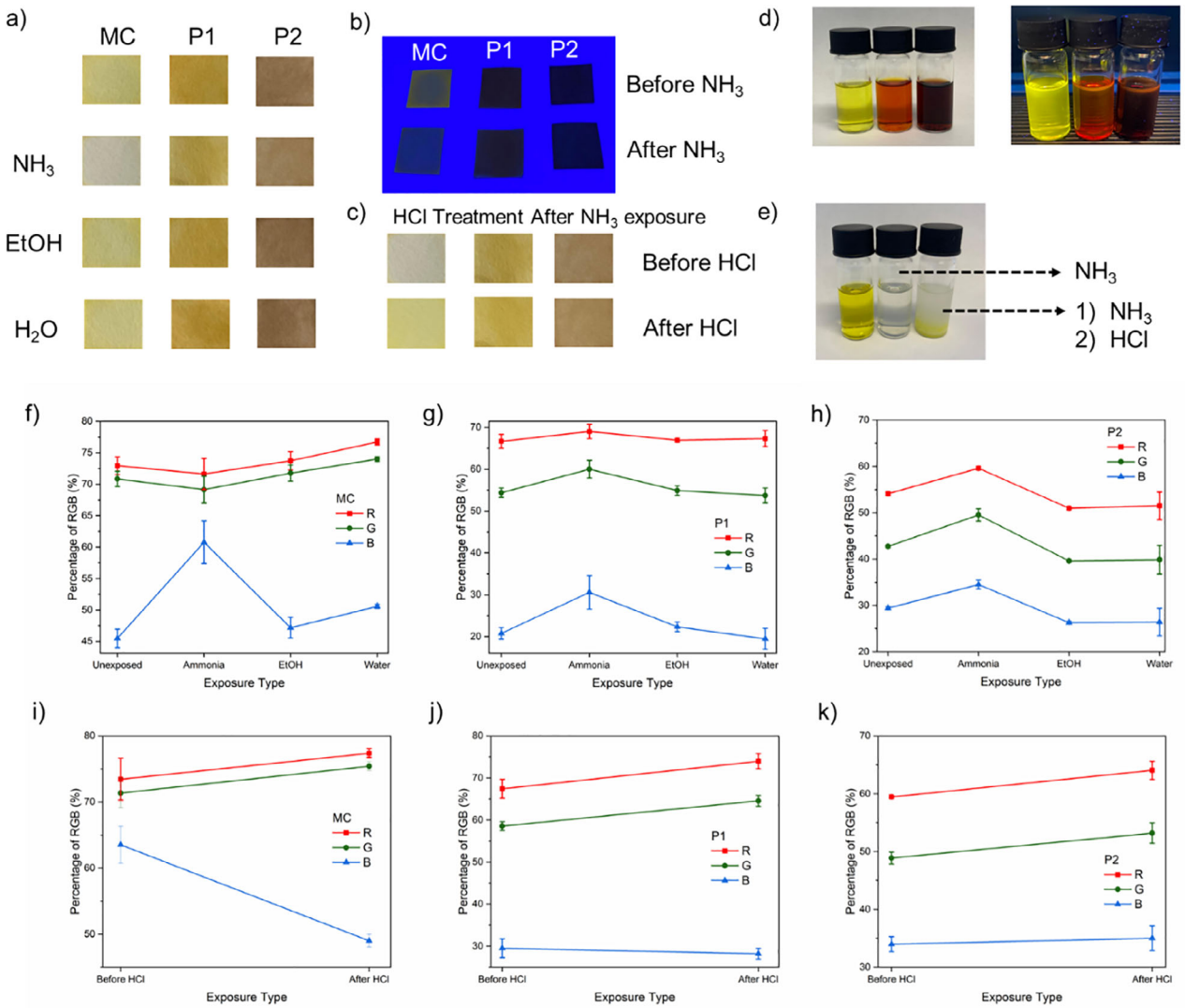

FIGURE 3 | Photographs of the paper-based colorimetric sensors: (a) under daylight, (b) under 366 nm UV light before and after NH_3 exposure, and (c) NH_3-exposed sensors after HCl treatment. Photographs of the synthesized sample solutions (MC: yellow, P1: light red, P2: dark red–each solution was prepared at 2 mg/mL in THF) under (d) daylight (left) and 366 nm UV light (right); (e) NH_3-exposed and HCl-treated MC sample. (f–k) RGB percentage values of the paper-based sensors upon exposure to different analytes. %RGB analysis performed from three different spots per image; average R, G, and B values were used for plotting. Error bars represent the standard deviation of the three readings.

3 | Conclusions

In conclusion, we have successfully synthesized and characterized MA-based conjugated materials using a greener, catalyst-free Perkin condensation route. Structural analyses via ^{1}H NMR and FTIR confirmed the formation of cyclic diaryl MA motifs, supported by distinctive spectral features. The synthesized materials were employed as colorimetric sensors for detecting ammonia and primary amines, showing a measurable decrease in π–π^* absorption transitions upon exposure to small amounts of (starting from 1 μL) ammonia or ethylamine. Furthermore, their application as paper-based colorimetric sensors demonstrated practical potential, with clear naked-eye color changes –particularly in the case of the smaller synthesized dye–indicating suitability for monitoring volatile ammonia and primary amine compounds. Finally, the materials exhibited reversible sensing behavior in the presence of acid vapors, allowing sensor recovery and multiple reuses, thereby contributing to a more sustainable sensing platform.

4 | Experimental Section

4.1 | Materials

Ac_2O (99%), ammonium hydroxide solution (30 wt.% in water), methylamine solution (40 wt.% in water), potassium hydroxide (KOH, pellets, >85%), pyruvic acid (98%), and 2,5-thiophendicarboxaldehyde (99%) were obtained from Sigma–Aldrich. 2-Me-THF, and terephtaldehyde were purchased from abcr GmbH, and diethylether (analytical grade) as well as absolute ethanol from VWR. HCl 37% fuming was purchased from Carl Roth. All chemicals were used without further

purification. Acetone-d_6, DMSO-d_6, and $CDCl_3$ were received acquired from Eurisotop or Carl Roth.

4.2 | Synthesis

For microwave syntheses, a Discover 2.0 microwave (CEM corporation, USA) was used.

4.3 | Characterizations

NMR measurements at room temperature were performed on an Avance III 500 spectrometer (^{1}H frequency 500.13 MHz, Bruker Corp., USA). High temperature NMR spectra were acquired using an Avance III 400 MHz spectrometer (^{1}H frequency 400.13 MHz, Bruker Corp., USA). Unless otherwise noted, all ^{1}H and ^{13}C NMR were acquired at room temperature. Polymer samples were heated to 80°C and kept at this temperature until complete dissolution in DMSO-d_6 was reached. NMR spectra of monomer samples were recorded in acetone-d6. MC NMR spectra were recorded in $CDCl_3$. IR measurements were conducted on an FTIR Spectrometer Vertex80v (Bruker Corp., USA) using a Golden Gate Diamond ATR Unit (SPECAC Ltd., UK) and an MCT-Detector. Wavenumbers between 4000 and 600 cm^{-1} were scanned. At a resolution of 4 cm^{-1}, 100 scans per measurement were completed. UV–vis measurements were carried out on a Cary 5000 UV–vis–NIR Spectrophotometer (Agilent Technologies Inc., USA). Wavelengths ranged between 800 and 280 nm. Liquid samples were prepared by dissolving the materials in THF (0.0625 mg/mL). $NH_{3(aq)}$ (30 wt.%) and water were added to the samples gradually. Solid samples were prepared by spin-coating as described above. Confocal microscopy of spin-coated films was measured with a μsurf expert device (Nanofocus AG, Germany). The magnification was set to 100 x, with a working distance of 0.3 mm. Surface sections with an area of 300 nm × 300 nm were scanned. The obtained data were processed and analyzed using the software μsoft metrology (Nanofocus AG, Germany).

4.4 | Synthesis of MC [17]

1.00 g (4.7 mmol) of starting materials for model compound (Potassium (*E*)-2-oxo-4-phenylbut-3-enoate (Scheme S1) and 0.516 g (2.6 mmol) of PDA were placed in a 25 mL RBF. Subsequently, 2 mL of acetic anhydride (Ac_2O) was added under an argon atmosphere. The reaction mixture was then heated to 120°C and maintained at that temperature for 1 h. During this period, the reaction suspension changed color from yellow to red. By the end of the 1-h reaction time, a red precipitate had formed. After cooling the reaction mixture to room temperature, the crude red product was collected by vacuum filtration. The remaining product in the RBF was extracted with 20 mL of acetone and filtered. The combined filtrates were washed thoroughly with 150 mL of acetone. The resulting orange solid was dried in an oven and collected. (Yield: 20%, 250 mg) ^{1}H NMR (300 MHz, CDCl3) δ 8.28 (d, J = 16.2 Hz, 1H), 7.87 (s, 2H), 7.62–7.54 (m, 1H), 7.47–7.39 (m, 2H), 7.19 (d, J = 16.2 Hz, 1H), 13C NMR (126 MHz, CDCl3) δ = 114.56, 127.19, 128.15, 129.03, 129.43, 130.63, 132.51, 134.37, 135.27, 144.51, 162.94, 163.46. The NMR spectrum is presented in (Figures S6 and S7).

4.5 | Synthesis of P1

A 10 mL microwave vial was charged with 54.9 mg M1 ((3*E*,3′*E*)-4,4′-(1,4-phenylene)bis(2-oxobut-3-enoic acid) 0.2 mmol, 1 eq.) and 38.8 mg PDA (0.2 mmol, 1 eq.), equipped with a stirring bar and set under a nitrogen atmosphere. To the starting materials, 1 mL acetic anhydride (3.24 g) and 2 mL anhydrous 2-Me-THF were added. The suspension was ultrasonicated for 10 min and irradiated in the microwave at 120°C for 2 h. After cooling to room temperature, the reaction mixture was poured onto 50 mL of diethylether and kept in the fridge overnight. The crude product was filtered off, washed with diethylether and dried under ambient conditions. (Yield: 40%, 32 mg). NMR and FTIR spectra are presented in (Figures S9–S11).

4.6 | Synthesis of P2

A 10 mL microwave vial was charged with 56.1 mg M2 ((3*E*,3′*E*)-4,4′-(thiophene-2,5-diyl)bis(2-oxobut-3-enoic acid), 0.2 mmol, 1 eq.) and 38.8 mg PDA (0.2 mmol, 1 eq.), equipped with a stirring bar and set under a nitrogen atmosphere. To the starting materials, 1 mL acetic anhydride (3.24 g) and 2 mL anhydrous 2-Me-THF were added. The suspension was ultrasonicated for 10 min and irradiated in the microwave at 120°C for 2 h. After cooling to room temperature, the reaction mixture was poured onto 50 mL of diethylether and kept in the fridge overnight. The crude product was filtered off, washed with diethylether and dried under ambient conditions (Yield: 45%, 37 mg). NMR and FTIR spectra are presented in (Figure S12).

4.7 | Thin Film Fabrication

For film production, the materials were spin-coated using an Ossila spin coater (Ossila Ltd., UK). As substrates, ultrathin quartz-coated glass slides (2 cm × 1.5 cm, Ossila Ltd., UK) were used. 2.5 mg/mL solutions of P1 and P2 in THF were prepared. The subsequent spin-coating was performed at room temperature using 80 μL of solution. The substrates were spun at 1000 rpm for 2 min.

4.8 | Fabrication of Paper-Based Sensors

Whatman Ashless 541 filter paper (70 mm diameter) was cut into 1 cm × 1 cm squares. Each sample solution (2 mg/mL in THF) was drop-cast onto the paper five times using 20 μL per application, allowing each layer to dry before adding the next. After the fifth application, the samples were dried completely and placed in glass petri dishes. The analytes were then introduced into the same Petri dishes by adding 20 μL of each analyte. Finally, RGB percentage analysis was performed on the captured images using *Paint.NET*.

5 | Statistics

For %RGB evaluation, three different spots were identified from each image, and the average R, G, and B values were calculated and used for plotting. Error bars represent the standard deviation

of these three readings. The σ value used for limit of detection (LOD) calculations was obtained from three UV/Vis measurements of the corresponding samples without analyte, determined as the standard deviation at the maximum absorbance.

Acknowledgments

We thank Dr. Mikhail Malanin for conducting IR experiments. R.T. additionally thanks Prof. Dr. Brigitte Voit for supervision and funding acquisition. Funded by the Deutsche Forschungsgemeinschaft (DFG, German Research Foundation) within GRK 2767 (Project number 451785257). Financial support by the Ingeborg-Gross Foundation is gratefully acknowledged. E.I. and F.L. also acknowledge funding by the European Union under grant agreement No. 101098996 "Flexible intelligent near-field sensing skins" (FITNESS). We thank Prof. Gerrit Luinstra (Institute of Technical and Macromolecular Chemistry, University of Hamburg) for hosting our research and for access to laboratory facilities, and Dr. Werner Pauer for helpful discussions and support. We also thank Prof. Jakob Albert (Institute of Technical and Macromolecular Chemistry, University of Hamburg) for providing access to laboratory facilities.

Funding

This work was funded by the Deutsche Forschungsgemeinschaft (DFG, German Research Foundation) within GRK 2767 (Project number 451785257). Financial support by the Ingeborg-Gross Foundation is gratefully acknowledged.

Conflicts of Interest

The authors declare no conflicts of interest.

Data Availability Statement

The data that support the findings of this study are available from the corresponding author upon reasonable request.

References

1. D. Wilkinson, D. Taylor, N. B. McKeown, and G. Cooke, "Bindone-based Polymer for Colorimetric Detection of Volatile Amines," *RSC Applied Polymers* 3, no. 3 (2025): 701–710, https://doi.org/10.1039/D5LP00017C.

2. J. Urbiña-Alvarez, S. Rincón-Carvajal, and D. Gamba-Sánchez, "Ammonia Surrogates in the Synthesis of Primary Amines," *Organic and Biomolecular Chemistry* 21, no. 35 (2023): 7036–7051.

3. W. Lv, J. Yang, Q. Xu, and J. A.-A. Mehrez, "Wide-range and High-accuracy Wireless Sensor with Self-humidity Compensation for Real-Time Ammonia Monitoring," *Nature Communication* 15, no. 1 (2024): 6936, https://doi.org/10.1038/s41467-024-51279-9.

4. S. Guthrie, S. Giles, and F. Dunkerley, *Impact of Ammonia Emissions from Agriculture on Biodiversity: An Evidence Synthesis* (RAND Corporation, 2018), https://doi.org/10.7249/RR2695.

5. M. J. Grant, A. Hoff, L. G. Kaake, and G. C. Welch, "Flexible Dual-action Colorimetric-Electronic Amine Sensors Based on N-Annulated Perylene Diimide Dyes," *Sensors and Diagnostics* 3, no. 5 (2024): 817–821.

6. T. Das, A. Pramanik, and D. Haldar, "On-line Ammonia Sensor and Invisible Security Ink by Fluorescent Zwitterionic Spirocyclic Meisenheimer Complex," *Scientific Reports* 7, no. 1 (2017): 40465, https://doi.org/10.1038/srep40465.

7. Z. Li and K. S. Suslick, "Portable Optoelectronic Nose for Monitoring Meat Freshness," *ACS Sensors* 1, no. 11 (2016): 1330–1335, https://doi.org/10.1021/acssensors.6b00492.

8. G. Singh, H. Singh, N. Kaur, and N. Singh, "Azodye-based Colorimetric Sensor Array for Identification of Biogenic Amines: Food Forensics by Portable RGB-Based Signal Readout," *Sensors and Actuators B: Chemical* 387 (2023): 133794.

9. S. H. Nah, J. B. Kim, H. N. T. Chui, Y. Suh, and S. Yang, "Enhanced Colorimetric Detection of Volatile Organic Compounds Using a Dye-Incorporated Photonic Crystal-Based Sensor Array," *Advanced Materials* 36, no. 46 (2024): 2409297, https://doi.org/10.1002/adma.202409297.

10. D. Kossyvaki, A. Barbetta, M. Contardi, et al., "Highly Porous Curcumin-Loaded Polymer Mats for Rapid Detection of Volatile Amines," *ACS Applied Polymer Materials* 4, no. 6 (2022): 4464–4475, https://doi.org/10.1021/acsapm.2c00418.

11. A. Lopera-Valle and A. Elias, "Colorimetric Indicators for Volatile Amines Based on Succinic Anhydride (SAh)-grafted Poly (lactic acid) (PLA)," *Analytical Methods* 12, no. 19 (2020): 2499–2508, https://doi.org/10.1039/D0AY00550A.

12. B. Liu, P. A. Gurr, and G. G. Qiao, "Irreversible Spoilage Sensors for Protein-Based Food," *ACS Sensors* 5, no. 9 (2020): 2903–2908, https://doi.org/10.1021/acssensors.0c01211.

13. Q. Zhang, L. Yu, W. Han, et al., "A Self-Calibrating Sensing Platform Based on Amine-Responsive Excitation Wavelength-Dependent Fluorescent Polymers for Real-Time and Visual Detection of Food Freshness," *Advanced Functional Materials* 34, no. 51 (2024): 2410000, https://doi.org/10.1002/adfm.202410000.

14. G. Das, B. Garai, T. Prakasam, et al., "Fluorescence Turn on Amine Detection in a Cationic Covalent Organic Framework," *Nature Communication* 13, no. 1 (2022): 3904, https://doi.org/10.1038/s41467-022-31393-2.

15. J. Yu and C. Zhang, "Fluorescent Sensing for Amines with a Low Detection Limit based on Conjugated Porous Polymers," *Journal of Material Chemistry C* 8, no. 46 (2020): 16463–16469, https://doi.org/10.1039/D0TC02592E.

16. J. Wang, D. Li, Y. Ye, et al., "A Fluorescent Metal–Organic Framework for Food Real-Time Visual Monitoring," *Advanced Materials* 33, no. 15 (2021): 2008020, https://doi.org/10.1002/adma.202008020.

17. E. K. Fields, S. J. Behrend, S. Meyerson, M. L. Winzenburg, B. R. Ortega, and H. K. Hall, "Diaryl-Substituted Maleic Anhydrides," *Journal of Organic Chemistry* 55, no. 17 (1990): 5165–5170, https://doi.org/10.1021/jo00304a034.

18. A. Robert, P. Dechambenoit, E. A. Hillard, H. Bock, and F. Durola, "Non-planar Oligoarylene Macrocycles from Biphenyl," *Chemical Communication* 53, no. 84 (2017): 11540–11543, https://doi.org/10.1039/C7CC06798D.

19. H. Böck, D. Subervie, P. Mathey, et al., "Helicenes from Diarylmaleimides," *Organic Letters* 16 (2014): 1546–1549.

20. A. Robert, P. Dechambenoit, H. Bock, and F. Durola, "A Carboxyfunctionalized (24)-1,6-pyrenophane-tetraene by Glyoxylic Perkin Condensation," *Canadian Journal of Chemistry* 95, no. 4 (2017): 450–453, https://doi.org/10.1139/cjc-2016-0585.

21. O. Stoilova, M. Ignatova, N. Manolova, T. Godjevargova, D. G. Mita, and I. Rashkov, "Functionalized Electrospun Mats from Styrene–Maleic Anhydride Copolymers for Immobilization of Acetylcholinesterase," *European Polymer Journal* 46, no. 10 (2010): 1966–1974, https://doi.org/10.1016/j.eurpolymj.2010.08.005.

22. S. Sun, C. Zhu, D. Song, F. Li, and A. Hu, "Preparation of Conjugated Polyphenylenes from Maleimide-Based Enediynes Through Thermal-Triggered Bergman Cyclization Polymerization," *Polymer Chemistry* 5, no. 4 (2014): 1241–1247, https://doi.org/10.1039/C3PY00970J.

23. H. Shih, R. J. Shih, and D. A. Carson, "New Heterocycles of 2,3-diaryl-substituted Maleic Hydrazides," *Journal of Heterocyclic Chemistry* 48, no. 6 (2011): 1243–1250, https://doi.org/10.1002/jhet.631.

24. A.-A. Zhang, Z.-X. Wang, Z.-B. Fang, J.-L. Li, and T.-F. Liu, "Long-Range π–π Stacking Brings High Electron Delocalization for Enhanced

Photocatalytic Activity in Hydrogen-Bonded Organic Framework," *Angewandte Chemical International Edition* 63, no. 46 (2024): e202412777, https://doi.org/10.1002/anie.202412777.

25. M. Xu, X. Li, Q. Zeng, and T. Zhang, "Synthesis and Study on Aggregation Behaviors in Liquid Phase of Three Prepared Cyanine Dyes," *Luminescence* 37, no. 10 (2022): 1733–1740, https://doi.org/10.1002/bio.4349.

26. L. Zhang and J. M. Cole, "Dye Aggregation in Dye-sensitized Solar Cells," *Journal of Materials Chemistry A* 5, no. 37 (2017): 19541–19559, https://doi.org/10.1039/C7TA05632J.

27. K. S. Gosavi, A. Patil, G. Wagh, G. H. Sonawane, A. Panigrahi, and D. K. Pal, "Rationally Designed Maleimide Dyes for Large Stokes Shifted Solvatochromism and Aggregation-Induced Emission," *Journal of Fluorescence* 35 (2025): 8417–8426, https://doi.org/10.1007/s10895-025-04172-7.

28. M.-H. Choi, E. J. Ko, Y. W. Han, E. J. Lee, and D. K. Moon, "Control of polymer-packing orientation in thin films through chemical structure of D-A type polymers and its application in efficient photovoltaic devices," *Polymer* 74 (2015): 205–215.

29. M. G. Khrenova, A. V. Nemukhin, and V. G. Tsirelson, "Origin of the π-stacking Induced Shifts in Absorption Spectral Bands of the Green Fluorescent Protein Chromophore," *Chemical Physics* 522 (2019): 32–38, https://doi.org/10.1016/j.chemphys.2019.02.010.

30. S. Ito, "Mechanochromic Luminescence of Soft Crystals: Recent Systematic Studies in Controlling the Molecular Packing and Mechanoresponsive Properties," *Journal of Photochemistry and Photobiology C: Photochemistry Reviews* 51 (2022): 100481, https://doi.org/10.1016/j.jphotochemrev.2021.100481.

31. Y.-Y. Zhou, Y.-C. Xu, Z.-F. Yao, et al., "Visualizing the Multi-level Assembly Structures of Conjugated Molecular Systems with Chain-length Dependent Behavior," *Nature Communication* 14, no. 1 (2023): 3340, https://doi.org/10.1038/s41467-023-39133-w.

32. K. Janus, D. Chlebosz, A. Janke, W. Goldeman, and A. Kiersnowski, "Contributions of Polymer Chain Length, Aggregation and Crystallinity Degrees in a Model of Charge Carrier Transport in Ultrathin Polymer Films," *Macromolecules* 56, no. 3 (2023): 964–973, https://doi.org/10.1021/acs.macromol.2c01998.

33. M. A. Tallon, "Reactions Involving Maleic Anhydride," in *Handbook of Maleic Anhydride Based Materials: Syntheses, Properties and Applications*, ed. O. M. Musa, (Springer International Publishing, 2016), 59–149, https://doi.org/10.1007/978-3-319-29454-4.

34. A. Lopera-Valle and A. Elias, "Amine Responsive Poly(lactic acid) (PLA) and Succinic Anhydride (SAh) Graft-Polymer: Synthesis and Characterization," *Polymers* 11 (2019): 1466.

35. P. Schmidt and S. Eschig, "An Industrial Applicable Method for the Synthesis of N-alkylated Maleimides Based on Fatty Amines," *European Journal of Lipid Science and Technology* 121, no. 1 (2019): 1800320, https://doi.org/10.1002/ejlt.201800320.

36. W. Liu, T. Liu, T. Liu, et al., "Improving Grafting Efficiency of Dicarboxylic Anhydride Monomer on Polylactic Acid by Manipulating Monomer Structure and Using Comonomer and Reducing Agent," *Industrial & Engineering Chemistry Research* 56, no. 14 (2017): 3920–3927.

37. Y. Jin, D. Du, C. Zhang, et al., "Modification of Poly(maleic anhydride)-Based Polymers with H2N–R Nucleophiles: Addition or Substitution Reaction?," *Bioconjugate Chemistry* 30, no. 3 (2019): 871–880, https://doi.org/10.1021/acs.bioconjchem.9b00008.

Supporting Information

Additional supporting information can be found online in the Supporting Information section.

Supporting File: adsr70154-sup-0001-SuppMat.docx.